

Migration transformation of two-dimensional magnetic vector and tensor fields

Michael S. Zhdanov,¹ Hongzhu Cai² and Glenn A. Wilson³

¹Department of Geology and Geophysics, University of Utah, 115 South, 1460 East, Room 383, Salt Lake City, UT 84112, USA, and TechnoImaging, 4001 South, 700 East, Suite 500, Salt Lake City, UT 84107, USA. E-mail: mzhdanov@technoimaging.com

²Department of Geology and Geophysics, University of Utah, 115 South, 1460 East, Room 383, Salt Lake City, UT 84112, USA

³TechnoImaging, 4001 South, 700 East, Suite 500, Salt Lake City, UT 84107, USA

Accepted 2012 March 8. Received 2012 March 8; in original form 2011 December 18

SUMMARY

We introduce a new method of rapid interpretation of magnetic vector and tensor field data, based on ideas of potential field migration which extends the general principles of seismic and electromagnetic migration to potential fields. 2-D potential field migration represents a direct integral transformation of the observed magnetic fields into a subsurface susceptibility distribution, which can be used for interpretation or as an *a priori* model for subsequent regularized inversion. Potential field migration is very stable with respect to noise in the observed data because the transform is reduced to the downward continuation of a well-behaved analytical function. We present case studies for imaging of SQUID-based magnetic tensor data acquired over a magnetite skarn at Tallawang, Australia. The results obtained from magnetic tensor field migration agree very well with both Euler deconvolution and the known geology.

Key words: Numerical solutions; Inverse theory; Magnetic and electrical properties; Australia.

1 INTRODUCTION

Magnetic vector data measured from orthogonal fluxgate magnetometers are dominated by the earth's background magnetic field, and are thus very sensitive to instrument orientation. Since their development in the 1960s, optically pumped magnetometers have been preferred for geophysical surveying as they directly measure the total magnetic intensity (TMI) and are insensitive to instrument orientation. Recently, SQUID-based sensors have been developed for directly measuring magnetic tensors (e.g. Schmidt *et al.* 2004; Stolz *et al.* 2006; Rompel 2009) which are advantageous for a number of reasons (Schmidt & Clark 2006). First, magnetic tensors are relatively insensitive to instrument orientation since magnetic gradients arise largely from localized sources and not the Earth's background field or regional trends. Secondly, magnetic tensor data obviate the need for base stations and diurnal corrections. Thirdly, the five independent components of the magnetic gradient tensor provide additional information regarding source location and magnetization directions, which is advantageous for the interpretation of under-samples surveys. Finally, remanent magnetization, including the Koenigsberger ratio, can be recovered from magnetic tensor data.

Given prior applications of SQUID-based systems for the real-time tracking of objects, magnetic tensor data have historically been interpreted by inversion for isolated sources (e.g. Wynn *et al.* 1975). While these methods may provide information about the sources, it

is not immediately obvious how that information can be prepared as an *a priori* susceptibility model for quantitative interpretation or a subsequent 3-D regularized inversion. In this paper, we present an alternative approach to rapid imaging of magnetic vector and tensor field data, one which is based on and extends the ideas of 2-D potential field migration as originally introduced by Zhdanov (2002), and gravity gradiometry migration, developed in Zhdanov *et al.* (2011).

Mathematically, migration is described by an action of the adjoint operator on the observed data. This concept has been long developed for seismic and electromagnetic wavefields (e.g. Schneider 1978; Berkhout 1980; Claerbout 1985; Zhdanov 1981, 1988, 2002) where the adjoint operators manifest themselves as the (back) propagation of seismic or electromagnetic fields in reverse time. When applied to potential fields, migration manifests itself as a special form of downward continuation of the potential field and/or its gradients (Zhdanov *et al.* 2011). A downward continuation is applied to the migration field which is obtained by relocating the sources of the observed field into the upper half-space as mirror images of the true sources. Contrary to conventional downward continuation of the potential field, downward continuation of the migration field is away from the mirror images of the sources. Therefore, migration is a stable transform, similar to upward continuation. At the same time, the migration field does contain remnant information about the original source distribution, which is why it can be used for subsurface imaging.

The advantage of potential field migration for geophysical applications is that it does not require any *a priori* information or assumptions about the type of the sources. In this paper, we provide a detailed exposition of potential field migration theory as applied to magnetic vectors and tensors in 2-D case, and demonstrate its application to GETMAG magnetic tensor data acquired over a magnetite skarn at Tallawang, Australia.

2 COMPLEX INTENSITY OF 2-D MAGNETIC VECTOR FIELDS

Consider a model with a 2-D distribution of magnetized regions with intensity of magnetization, $\mathbf{I}(x, z) = (I_x(x, z), I_z(x, z))$, within a domain, Γ (Fig. 1). As per Zhdanov (1988), the magnetic field can be expressed as:

$$\mathbf{H}(x', z') = 2\tilde{\nabla}' \iint_{\Gamma} \mathbf{I}(x, z) \cdot \frac{(x - x')\mathbf{d}_x + (z - z')\mathbf{d}_z}{(x - x')^2 + (z - z')^2} ds, \quad (1)$$

where $\tilde{\nabla}'$ denotes a 2-D differential operator, $\tilde{\nabla}' = (\partial/\partial x', \partial/\partial z')$, and \mathbf{d}_x and \mathbf{d}_z are the unit basis vectors of the Cartesian system of coordinates. We can define the complex intensity of magnetization as:

$$I(\zeta) = I_x(x, z) + iI_z(x, z). \quad (2)$$

It follows that the complex intensity of the magnetic field can be defined as:

$$\begin{aligned} H(\zeta') &= -H_x(x', z') + iH_z(x', z') \\ &= A^H(I) = -2 \iint_{\Gamma} \frac{1}{(\zeta - \zeta')^2} I(\zeta) ds, \end{aligned} \quad (3)$$

where $\zeta = x + iz$, and A^H denotes the modelling operator of the magnetic field in terms of the complex intensity of magnetization. As described by Zhdanov (1988), the complex intensity of the magnetic field satisfies the following equation:

$$\frac{\partial}{\partial \zeta'^*} H(\zeta) = 2I(\zeta). \quad (4)$$

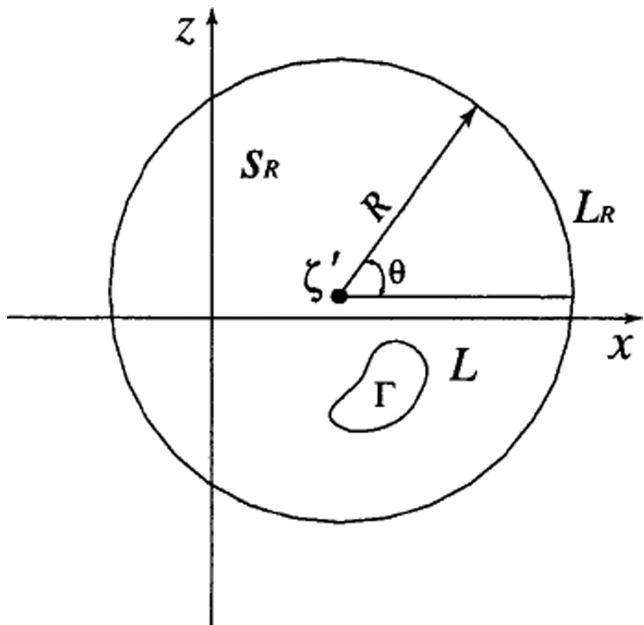


Figure 1. A complex plane describing the 2-D magnetic problem.

In what follows, we adopt the common assumption that there is no remanent magnetization, that self-demagnetization effects are negligible, and that the magnetic susceptibility is isotropic. Under this assumption, the intensity of magnetization is given as a product of the magnetic susceptibility $\chi(x, z)$, the strength of the inducing magnetic field, H_o , and a unit vector \mathbf{l} ; i.e. defining the direction of the inducing magnetic field. The intensity of magnetization can be expressed via the 2-D distribution of magnetic susceptibility, $\chi(x, z)$, as:

$$I_x(x, z) = H_o\chi(x, z) \cos \theta; \quad I_z(x, z) = H_o\chi(x, z) \sin \theta, \quad (5)$$

where H_o is magnetic induction and θ is the angle of magnetization which is the angle between the vector \mathbf{l} and horizontal axis x .

Now, consider that $\zeta = x + iz$ and $\zeta' = x' + iz'$. The magnetic field along the horizontal axis $z' = 0$, according to eqs (3) and (5), can be written as:

$$\begin{aligned} H(\zeta') &= -2 \iint_{\Gamma} \frac{1}{(\zeta - \zeta')^2} I(\zeta) ds \\ &= -2 \iint_{\Gamma} \frac{(\cos \theta + i \sin \theta) H_o \chi}{(x - x' + iz)^2} ds'. \end{aligned} \quad (6)$$

Eq. (6) can be used for modelling magnetic field data.

3 COMPLEX INTENSITY OF 2-D MAGNETIC TENSOR FIELDS

The second spatial derivatives of the magnetic potential form a symmetric *magnetic tensor*:

$$\hat{\mathbf{H}} = \begin{bmatrix} H_{xx} & H_{xz} \\ H_{zx} & H_{zz} \end{bmatrix},$$

with zero trace, where:

$$H_{\alpha\beta} = \frac{\partial H_{\alpha}}{\partial \beta}, \quad \alpha, \beta = x, z. \quad (7)$$

We define the complex intensity of the magnetic tensor field, $H_T(\zeta)$, as a complex derivative of the complex intensity of the magnetic field, $H(\zeta)$:

$$H_T(\zeta) = \frac{\partial H(\zeta)}{\partial \zeta} = \frac{1}{2} \left(\frac{\partial}{\partial x} - i \frac{\partial}{\partial z} \right) H(\zeta). \quad (8)$$

Substituting eq. (3) into (8), we find that:

$$H_T(\zeta) = H_{zz}(x, z) + iH_{zx}(x, z), \quad (9)$$

which takes into account the symmetry of the magnetic tensor, i.e. $H_{zx} = H_{xz}$, and the fact that magnetic potential outside the sources should satisfy Laplace's equation:

$$H_{xx}(x, z) + H_{zz}(x, z) = 0. \quad (10)$$

According to eqs (6) and (8), we have the following expression for the complex intensity of the magnetic tensor field:

$$H_T(\zeta') = A^T(I) = -4 \iint_{\Gamma} \frac{1}{(\zeta - \zeta')^3} I(\zeta) ds, \quad \zeta' \notin \Gamma, \quad (11)$$

where $A^T(I)$ denotes the modelling operator of the magnetic tensor field in terms of the complex intensity of magnetization. As for the magnetic vector field, we can express the magnetic tensor field in terms of magnetic susceptibility, $\chi(x, z)$, and the angle of

magnetization, θ :

$$\begin{aligned} H_T(\zeta') &= -4 \iint_{\Gamma} \frac{1}{(\zeta - \zeta')^3} I(\zeta) ds \\ &= -4 \iint_{\Gamma} \frac{(\cos \theta + i \sin \theta) H_o \chi}{(x - x' + iz)^3} ds \\ &= H_{zz}(x, z) + i H_{zx}(x, z). \end{aligned} \quad (12)$$

Eq. (12) can be used for modelling magnetic tensor data.

Note that both the complex intensities of the magnetic field $H(\zeta')$ and the magnetic tensor field $H_T(\zeta')$ are described by analytical functions outside the masses, i.e. $\zeta' \notin \Gamma$. As will become apparent in subsequent sections of this paper, the analytical representations for the magnetic vector and tensor fields will serve a useful purpose for the solution of their corresponding inverse problems.

4 ADJOINT OPERATORS OF COMPLEX MAGNETIC VECTOR AND TENSOR FIELDS

Mathematically, migration is the action of the adjoint operator upon the observed data. The closed form of the adjoint operator for a complex 2-D magnetic potential was first developed by Zhdanov (2002). We will extend this derivation to 2-D magnetic vector and tensor fields.

Let us assume that we have observed magnetic field, $H(\zeta')$, along a line of observations, L . The domain, Γ , which is filled with the masses generating the observed field, is located in the lower half-plane. We introduce a complex Hilbert space, D , of magnetic data with the metric:

$$(H, f)_D = \int_L H(\zeta') f^*(\zeta') d\zeta'; \quad H, f \in D, \quad (13)$$

and a real Hilbert space, M , of models (i.e. magnetic susceptibility, $\chi(\zeta)$) with the metric:

$$(\eta, \chi)_M = \iint_{\Gamma} \eta(\zeta) \chi(\zeta) ds; \quad J, \chi \in M. \quad (14)$$

We will derive an explicit form of the adjoint operator, A^{H*} , for the magnetic field such that for any function, $f(x')$:

$$(A^H(\chi), f)_D = (\chi, A^{H*}(f))_M. \quad (15)$$

Using the definitions (13) and (14) of the inner products, and eq. (6) for the modelling operator of the magnetic field, we can rewrite eq. (15) as:

$$\begin{aligned} (A^H(\chi), f)_D &= \int_{-\infty}^{\infty} A^H(\chi) f^* dx' \\ &= -(\chi, 2 \int_{-\infty}^{\infty} \frac{(\cos \theta + i \sin \theta) H_o f^*(x')}{(\zeta - x')^2} dx')_M = (\chi, A^{H*}(f))_M, \end{aligned} \quad (16)$$

where the asterisk, $*$, denotes the complex conjugate.

From eq. (16), we can find the following identity:

$$\left(\chi, A^{H*}(f) + 2 \int_{-\infty}^{\infty} \frac{(\cos \theta + i \sin \theta) H_o f^*(x')}{(\zeta - x')^2} dx' \right)_M = 0. \quad (17)$$

Since identity (17) holds for any $\chi(\zeta)$, we find that the adjoint magnetic operator, A^{H*} , applied to any function $f(x')$ is given by:

$$A^{H*}(f) = -2 \int_{-\infty}^{\infty} \frac{(\cos \theta + i \sin \theta) H_o f^*(x')}{(\zeta - x')^2} dx'. \quad (18)$$

From a derivation similar to the one given above, we can find that the adjoint magnetic tensor operator, A^{T*} , applied to any function $f(x')$, is given by:

$$A^{T*}(f) = -4 \int_{-\infty}^{\infty} \frac{(\cos \theta + i \sin \theta) H_o f^*(x')}{(\zeta - x')^3} dx'. \quad (19)$$

Note that both the adjoint operators for magnetic vector and tensor fields generate analytical functions. As will become apparent in subsequent sections of this paper, these analytical representations will serve a useful purpose for the solution of their corresponding inverse problems.

5 ADJOINT FIELDS AND THEIR RELATIONSHIP WITH THE MAGNETIC AND TENSOR FIELD MIGRATIONS

Let us analyze the result of applying the adjoint magnetic operator to a magnetic field, H_{Γ} , observed on the x axis:

$$A^{H*} H_{\Gamma} = -2 \int_{-\infty}^{\infty} \frac{(\cos \theta + i \sin \theta) H_o H_{\Gamma}^*(x')}{(\zeta - x')^2} dx'. \quad (20)$$

Let us study the physical meaning of this last equation. First, we examine the expression for $H_{\Gamma}^*(x')$. According to eq. (6), we can see that:

$$\begin{aligned} H_{\Gamma}^*(x') &= -2 \iint_{\Gamma} \frac{1}{(\zeta^* - x')^2} I^*(\zeta) ds \\ &= -2 \iint_{\Gamma^*} \frac{1}{(\zeta - x')^2} I^*(\zeta^*) ds = H_{\Gamma^*}(x'), \end{aligned} \quad (21)$$

where $H_{\Gamma^*}(x')$ can be treated as the magnetic field of the magnetic sources located in domain Γ^* , which is a mirror image of domain Γ with respect to the x axis (Fig. 2). We call H_{Γ^*} the *adjoint magnetic field*. The complex intensity of magnetization $\tilde{I}(\zeta)$ within Γ^* is a complex conjugate mirror image of the intensity of magnetization distribution $I(\zeta)$ in Γ , i.e. $\tilde{I}(\zeta) = I^*(\zeta^*)$. Obviously, the adjoint magnetic field, H_{Γ^*} , is an analytical function everywhere in the lower half-plane, and can be expressed as:

$$H_{\Gamma^*}(\zeta) = -2 \iint_{\Gamma^*} \frac{1}{(\zeta - \tilde{\zeta})^2} \tilde{I}(\tilde{\zeta}) d\tilde{s}, \quad \zeta \notin \Gamma^*, \quad z < 0, \quad (22)$$

where $\tilde{\zeta} = \tilde{x} + i\tilde{z} \in \Gamma^*$ is a variable of integration, and $d\tilde{s} = d\tilde{x}d\tilde{z}$.

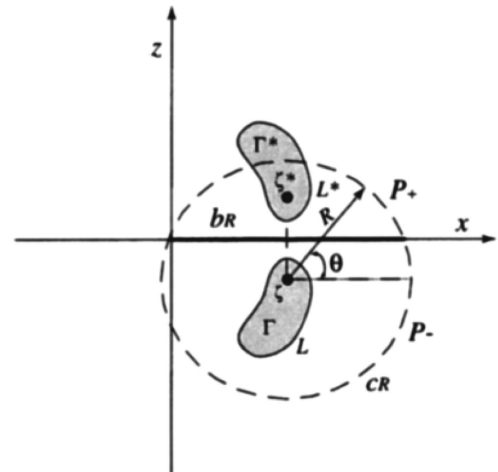


Figure 2. Definition of the adjoint magnetic vector, H_{Γ^*} . The field H_{Γ^*} is generated by the sources located in Γ^* . The magnetic susceptibility distribution $\tilde{\chi}(\zeta)$ within Γ^* is a mirror image of the magnetic susceptibility distribution $\chi(\zeta)$ in Γ : $\tilde{\chi}(\zeta) = \chi(\zeta^*)$.

Now, let us consider Fig. 2. Let P^+ stand for the upper half-plane of a complex plane ζ , bounded by the real axis x , and P^- for the lower half-plane. We consider an arbitrary point $\zeta \in \Gamma$ and draw therefrom a circle of radius, R . That part of the real axis X that happens to lie inside the circle will be represented by b_R , while that part of the circle found inside P^- will be denoted by C_R . According to the Cauchy integral formula, we have the following relationship:

$$H_{\Gamma^*}(\zeta) = \frac{1}{2\pi i} \int_{b_R} \frac{H_{\Gamma^*}(\zeta')}{\zeta' - \zeta} d\zeta' + \frac{1}{2\pi i} \int_{C_R} \frac{H_{\Gamma^*}(\zeta')}{\zeta' - \zeta} d\zeta', \quad \zeta \in P^-, \tag{23}$$

where the integration over the closed contour $b_R \cup C_R$ is taken in the counter-clockwise direction. In particular, the integration over the segment b_R of the real axis is from right to left. Now, let radius R go to infinity. The integral over semicircle C_R would become zero as $R \rightarrow \infty$, because the function $H_{\Gamma^*}(\zeta)$, being analytical, tends uniformly to zero at infinity. Therefore, eq. (23) takes the form:

$$H_{\Gamma^*}(\zeta) = -\frac{1}{2\pi i} \int_{-\infty}^{\infty} \frac{H_{\Gamma^*}(x')}{x' - \zeta} dx', \quad \zeta \in P^-, \tag{24}$$

where $H_{\Gamma^*}(x')$ is the magnetic field generated along the x axis by the magnetic sources located in domain Γ^* , and the minus sign arises because we have changed the direction of integration; it is now conducted from the left ($-\infty$) to the right ($+\infty$).

According to eq. (21), we have the following relationship:

$$H_{\Gamma^*}(x') = H_{\Gamma^*}^*(x'). \tag{25}$$

As a result, eq. (24) can be rewritten as follows:

$$H_{\Gamma^*}(\zeta) = -\frac{1}{2\pi i} \int_{-\infty}^{\infty} \frac{H_{\Gamma^*}^*(x')}{x' - \zeta} dx', \quad \zeta \in P^-. \tag{26}$$

Note that, there is a close resemblance between eq. (26) and the definition of the Hilbert transform of a real function of a real variable [although eq. (26) involves complex variables]. In the case of the conventional Hilbert transform, the observation point ζ usually belongs to the line of integration, which results in the singularity of the kernel $1/(x' - \zeta)$ at this point. In our case, we assume that point ζ is located inside P^- , thus avoiding any singularity.

Taking into account eq. (26), we can represent eq. (20) in the following form:

$$A^{H^*} H_{\Gamma} = -4\pi i (\cos \theta + i \sin \theta) H_o \frac{\partial}{\partial \zeta} H_{\Gamma^*}(\zeta). \tag{27}$$

Thus, we see that the application of the adjoint magnetic operator to an observed magnetic field is equivalent to taking a derivative of the analytical continuation of the adjoint magnetic field in the lower half-plane. Following Zhdanov (2002), we will call this transformation a *magnetic vector migration*, and use the notation:

$$H_{\Gamma}^m(\zeta) = A^{H^*} H_{\Gamma}, \tag{28}$$

where H_{Γ}^m is called the *migration magnetic field*.

In a similar way, the *migration magnetic tensor field*, $H_T^m(\zeta)$, is introduced as a result of application of the adjoint operator, A_T^* , to the complex intensity, $H_T(\zeta)$, of the observed magnetic tensor field:

$$H_T^m(\zeta) = A_T^* H_T. \tag{29}$$

Note that, the complex conjugate of the complex intensity of the magnetic tensor, H_T^* , satisfies equations similar to eqs (25) and (26), i.e.:

$$H_T^*(x') = H_T^*(x'), \tag{30}$$

$$H_{T^*}(\zeta) = -\frac{1}{2\pi i} \int_{-\infty}^{\infty} \frac{H_T^*(x')}{x' - \zeta} dx', \quad \zeta \in P^-, \tag{31}$$

where $H_{T^*}(\zeta)$ is the *adjoint magnetic tensor field* generated by the magnetic sources located in domain Γ^* .

Taking into account eqs (29) and (19), we can write:

$$H_T^m(\zeta) = 2\pi i (\cos \theta + i \sin \theta) H_o \frac{\partial^2}{\partial \zeta^2} H_{T^*}(\zeta). \tag{32}$$

Thus, we see that the migration of the observed magnetic tensor field, H_T , is equivalent to taking the second derivative of the analytical continuation of the adjoint magnetic tensor field, H_{T^*} , in the lower half-plane. Physically, this indicates that magnetic tensors have a higher sensitivity to magnetization than magnetic vectors.

6 MIGRATION IMAGING OF MAGNETIC FIELD DATA

It is very well known that the adjoint operator plays an important role in imaging and the solution of inverse problems (Zhdanov 2002). However, direct application of the adjoint operators to observed data does not produce an adequate image of the subsurface. It was shown by Zhdanov (2002) that, in order to image sources at their correct locations, one should apply an appropriate spatial weighting operator to the migration field. This weighting operator is constructed based on the integrated sensitivity of the data to the model parameters.

For example, the weighting operator W_H for the magnetic inverse problem is the linear operator of multiplication by functions w_H that are equal to the square root of the integrated sensitivity of the complex intensity of the magnetic field, S_H :

$$w_H = \sqrt{S_H}, \tag{33}$$

where the integrated sensitivity of the magnetic vector field is calculated by the following formula:

$$S_H = H_o \sqrt{\frac{2\pi}{|z|^3}}, \quad z < 0. \tag{34}$$

Using the same approach as one discussed in Zhdanov (2002) and Zhdanov *et al.* (2011) for gravity field, we can find the first approximation for the distribution of magnetic susceptibility, described by the following expression:

$$\begin{aligned} \chi^H(\zeta) &= w_H^{-1}(z) \chi_1^w = k_H w_H^{-1}(z) \operatorname{Re} A_w^{H^*} (H_{\Gamma}) \\ &= k_H w_H^{-2}(z) \operatorname{Re} A_w^{H^*} (H_{\Gamma}) = k_H w_H^{-2}(z) \operatorname{Re} H_{\Gamma}^m(\zeta), \end{aligned} \tag{35}$$

where

$$k_H = \frac{\|A_w^{H^*} H_{\Gamma}\|_M^2}{\|A_w^H A_w^{H^*} H_{\Gamma}\|_D^2}. \tag{36}$$

The magnetic susceptibility defined by eq. (35) is called a *migration susceptibility* and it is denoted as $\chi_m^H(\zeta)$:

$$\chi_m^H(\zeta) = \chi^H(\zeta) = k_H w_H^{-2}(z) \operatorname{Re} H_{\Gamma}^m(\zeta), \tag{37}$$

where $\zeta' = x' + iz'$. It is proportional to the weighted real part of the migration magnetic field, H_{Γ}^m .

Thus, migration with spatial weighting provides a stable algorithm for calculating the migration susceptibility. Substituting

eq. (20) into (28) and (37), after some algebra, we finally find:

$$\begin{aligned} \chi_m(x, z) &= 2k_0^w w_H^{-2}(z) \int_{-\infty}^{\infty} \frac{(\cos \theta H_x - \sin \theta H_z)[(x-x')^2 - z^2]}{[(x-x')^2 + z^2]^2} H_o dx' \\ &+ 4k_0^w w_H^{-2}(z) \int_{-\infty}^{\infty} \frac{(\sin \theta H_x + \cos \theta H_z)(x-x')z}{[(x-x')^2 + z^2]^2} H_o dx'. \end{aligned} \quad (38)$$

7 MIGRATION IMAGING OF MAGNETIC TENSOR FIELD

The migration magnetic tensor field, $H_T^m(\zeta)$, was introduced above as a result of application of the adjoint operator, A_T^* , to the complex intensity, $H_T(\zeta)$, of the observed tensor field:

$$H_T^m(\zeta) = A_T^* H_T, \quad (39)$$

where according to eq. (19)

$$A_T^* H_T = -4 \int_{-\infty}^{\infty} \frac{(\cos \theta + i \sin \theta) H_o H_T^*(x')}{(\zeta - x')^3} dx'. \quad (40)$$

As for magnetic field, we can introduce a migration magnetic susceptibility based on the magnetic tensor migration:

$$\chi_m^T(\zeta) = k_{T0} w_T^{-2}(z) A_T^* H_T = k_{T0} w_T^{-2}(z) H_T^m(\zeta), \quad (41)$$

where:

$$k_T = \frac{\|A_T^{w*} H_T\|_M^2}{\|A_T^w A_T^{w*} H_T\|_D^2}, \quad (42)$$

$$A_T^w = A_T W_T^{-1}. \quad (43)$$

As usual, the weighting function w_T is selected to be equal to the square root of the integrated sensitivity of the magnetic tensor field, S_T :

$$w_T = \sqrt{S_T}, \quad (44)$$

where the integrated sensitivity of the magnetic tensor field is calculated by the following equation:

$$S_T = H_o \sqrt{\frac{6\pi}{|z|^5}}, \quad z < 0. \quad (45)$$

Finally, for the magnetic tensor fields, we can find the expression of the migration magnetic susceptibility as:

$$\begin{aligned} \chi_m^T &= -4k_0^w w_T^{-2}(z) \\ &\times \int_{-\infty}^{\infty} \frac{(\cos \theta H_{zz} + \sin \theta H_{zx})[(x-x')^3 - 3(x-x')z^2]}{[(x-x')^2 + z^2]^3} H_o dx', \\ &- 4k_0^w w_T^{-2}(z) \int_{-\infty}^{\infty} \frac{(\sin \theta H_{zz} - \cos \theta H_{zx})[3(x-x')^2z - z^3]}{[(x-x')^2 + z^2]^3} H_o dx'. \end{aligned} \quad (46)$$

8 MODEL STUDIES

To demonstrate the effectiveness of 2-D potential field migration for both magnetic vector and tensor data, we first consider two synthetic 2-D models. The first synthetic model consists of a rectangular body of 100 m width and 300 m depth, buried 400 m below the surface. The susceptibility of the body is 0.4 SI and it is embedded in an otherwise homogeneous and non-magnetic host. The inducing magnetic field has an inclination of 45 degrees, and we contaminated both vector and tensor data with random Gaussian noise equal to

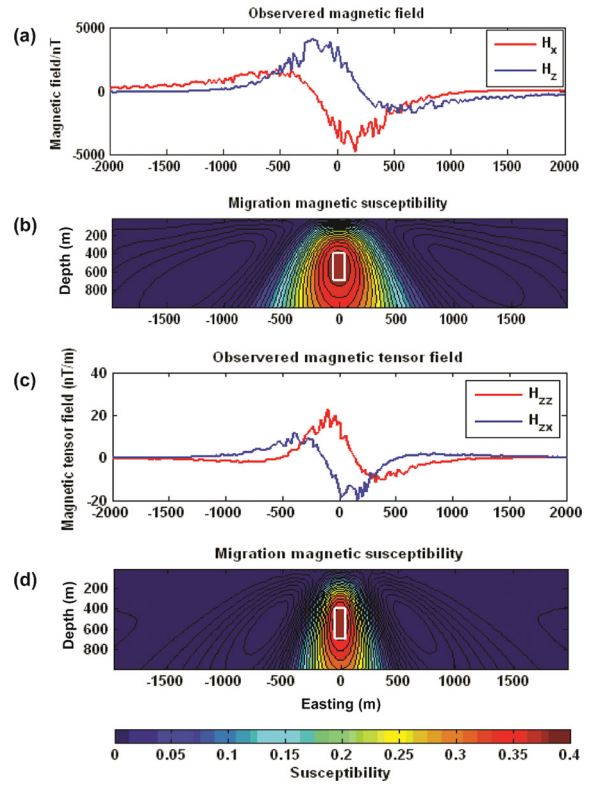


Figure 3. (a) Synthetic magnetic vector (H_x and H_z) data with 30 per cent noise for single body with 0.4 susceptibility. (b) Magnetic vector migration image. (c) Synthetic magnetic tensor (H_{zz} and H_{zx}) data with 30 per cent noise for single body with 0.4 susceptibility. (d) Magnetic tensor migration image.

30 per cent of the signal of each component. The results are shown in Fig. 3. As can be seen, the body is recovered from both vector and tensor migrations; as expected, the latter provides a more compact image of the body.

The second synthetic model consists of two square bodies of 200 m dimension; one at 300 m depth, and the other at 400 m depth. The susceptibility of both bodies is 0.4 SI. They are embedded in an otherwise homogeneous and non-magnetic host. The inducing magnetic field has an inclination of 45 degrees, and we contaminated both vector and tensor data with 30 per cent random noise. The results are shown in Fig. 4. Again, both bodies are recovered from both vector and tensor migrations; and as expected, the latter provides a more compact image of the bodies.

It is important to emphasize that migration suppresses the effect of the noise on the data and provides a correct image of the target even in a case of 30 per cent random noise. These examples illustrate the fact that migration is indeed a very stable transformation.

9 CASE STUDY

The most appropriate sensors for measuring magnetic tensors are superconducting quantum interference devices (SQUIDs), which detect minute changes of flux threading a superconducting loop. They are therefore variometers rather than magnetometers, but they are vector sensors since only changes perpendicular to the loop are detected (Foley & Leslie 1998; Foley *et al.* 1999; Lee *et al.* 2001). Based on Tilbrook (2004), a manually rotated prototype of CSIRO's GETMAG magnetic gradiometer (Schmidt *et al.* 2004) is an

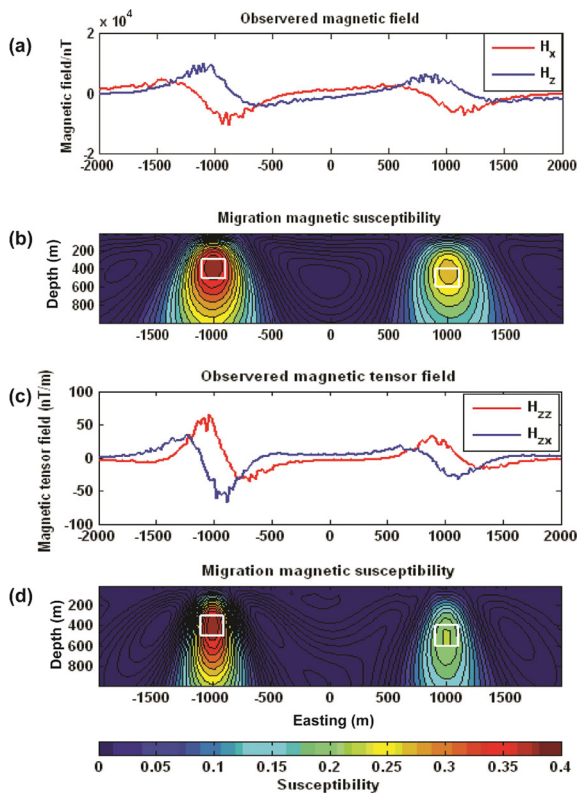


Figure 4. (a) Synthetic magnetic vector (H_x and H_z) data with 30 per cent noise for two bodies with 0.4 susceptibility. (b) Magnetic vector migration image. (c) Synthetic magnetic tensor (H_{zz} and H_{zx}) data with 30 per cent noise for two bodies with 0.4 susceptibility. (d) Magnetic tensor migration image.

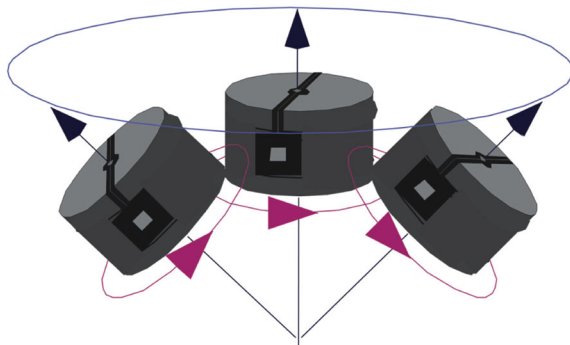


Figure 5. Schematic of CSIRO's GETMAG sensor configuration with the three rotating SQUID sensors in an umbrella configuration (from Schmidt *et al.* 2004).

integrated package of three rotating single-axial gradiometer sensors in an umbrella arrangement, as shown in Fig. 5. This configuration has several distinct advantages. First, it reduces the required number of sensors and electronics. Secondly, the amount of crosstalk between sensors is reduced by employing different rotation frequencies. This shifts the measurement (rotation) frequency from quasi-DC to tens or hundreds of hertz, leading to a reduced intrinsic sensor noise and a reduced influence of low frequency mechanical vibrations; thus, the requirements for a suspension system for airborne deployment are significantly reduced. Thirdly, by implementing data extraction through Fourier analysis, magnetic vectors

can be separated from magnetic tensors as the signals are centered at the fundamental and at twice the rotation frequency, respectively. Thus, with only three single-axial sensors, all vector and tensor components can be recovered.

Schmidt *et al.* (2004) demonstrated CSIRO's GETMAG system with a field trial of three profiles (50, 60 and 120 mN) over a magnetite skarn deposit at Tallawang, near Gulgong in New South Wales, Australia. The deposit is roughly tabular, striking north-north-west and dipping steeply to the west. The survey was approximately perpendicular to strike, minimizing aliasing and effectively making the surveys 2-D. The Tallawang magnetite skarn is located along the western margin of the Gulgong Granite, which was intruded during the Kanimblan Orogeny in the Late Carboniferous. In detail, the magnetite occurs in lenses thought to reflect replacement of a tightly folded host rock sequence (Tucklan Beds), and is additionally complicated by transverse faulting, causing east-west displacement of the magnetite zones. The magnetite body is well delineated by numerous drill holes and the rock magnetic properties of the magnetite have been well characterized. The strongest samples possessed susceptibility of 3.8 SI (0.3 cgs) and remanence of 40 Am^{-1} , yielding Königsberger ratios between 0.2 and 0.5. The mean direction of the remanence is west-north-west and steeply up. This direction may be the result of a dominant viscous remanent magnetization in the direction of the recent geomagnetic field, and a reversed mid-Carboniferous component, dating from the time that the Gulgong Granite was intruded. The effective magnetization, projected onto a vertical plane perpendicular to strike, is directed steeply upwards.

We have applied magnetic tensor migration to the three profiles of GETMAG H_{zz} and H_{zx} data to obtain 2-D susceptibility images. Figs 6, 7 and 8 show the observed data and migration images for each of the GETMAG profiles. In each of the figures, the background is

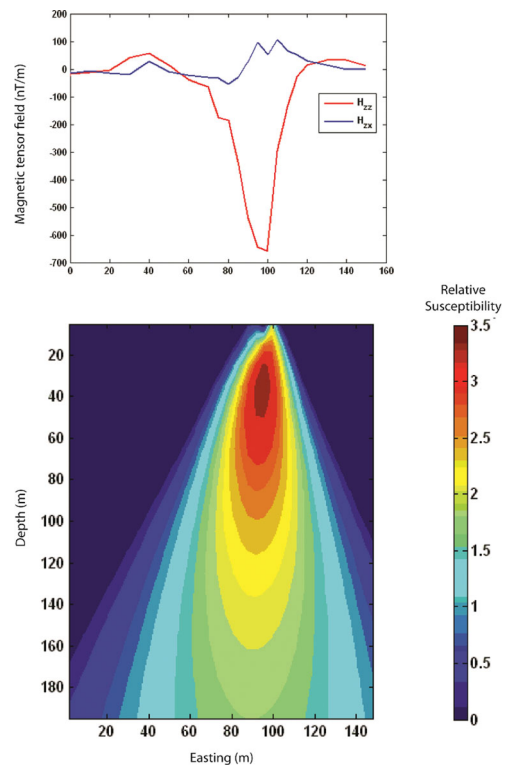


Figure 6. Magnetic tensor migration for GETMAG components H_{zz} and H_{zx} measured on line 50 mN over the Tallawang magnetite skarn.

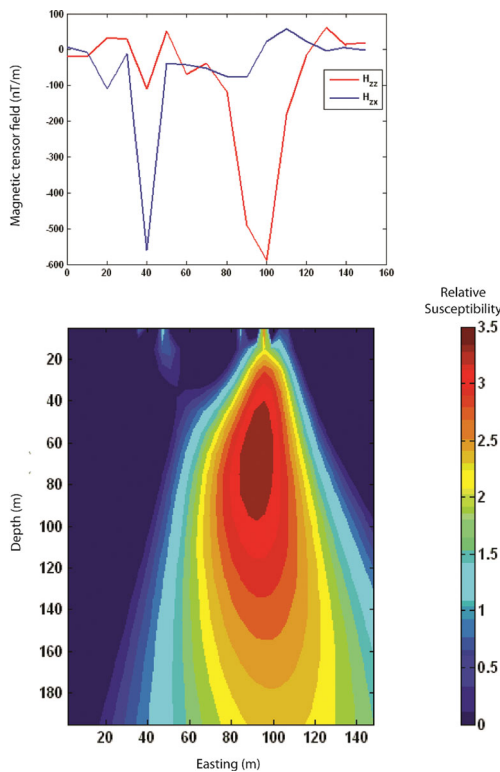


Figure 7. Magnetic tensor migration for GETMAG components H_{zz} and H_{zx} measured on line 60 mN over the Tallawang magnetite skarn. The anomaly at 40 m E corresponds to a steel drill collar at the surface.

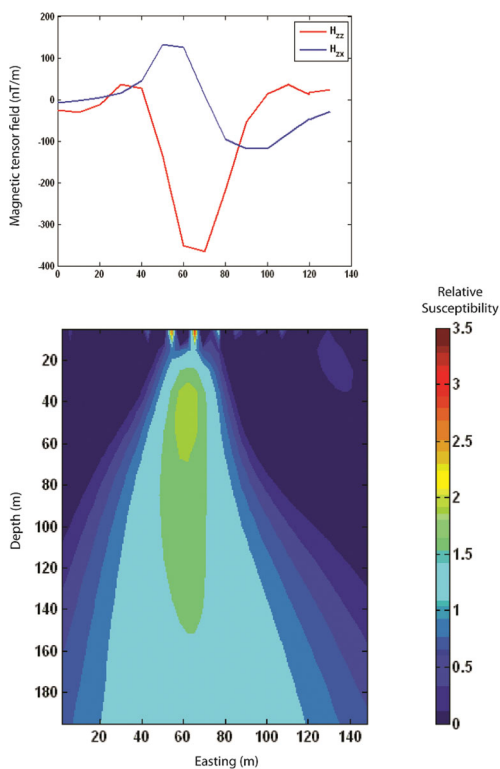


Figure 8. Magnetic tensor migration for GETMAG components H_{zz} and H_{zx} measured on line 120 mN over the Tallawang magnetite skarn.

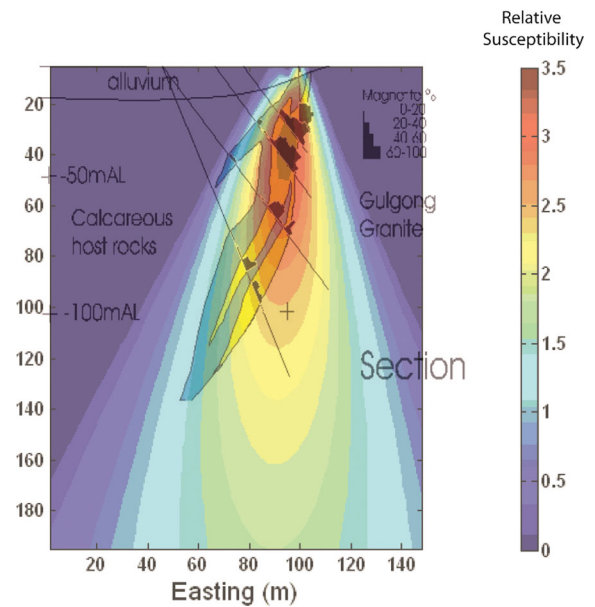


Figure 9. Inferred geology of the Tallawang magnetite skarn superimposed on the magnetic tensor migration image for GETMAG components H_{zz} and H_{zx} measured on line 50 mN.

dominated by uniformly magnetized strata (i.e. no external magnetic expression). The magnetite skarn deposit is recovered as a dike-like body whose top is about 10 m deep, with a maximum susceptibility at approximately 30 m depth; most probably fresh, unweathered magnetite with significant magnetization in contrast to the mantle of the weathered skarn. These results are in very good agreement with those obtained from Euler deconvolution (Schmidt *et al.* 2004) and the known geology (Fig. 9). We note that our migration result is inherently 2-D, meaning that local (e.g. 3-D) strike could not be recovered; thus the fault between profiles 60 and 120 mN is not identified. However local strike information is readily derived from eigenvector analysis of the gradient tensor (Schmidt *et al.* 2004).

10 CONCLUSIONS

We have introduced the theory of 2-D potential field migration and demonstrated its application to the imaging of magnetic vector and tensor data. We have shown that magnetic migration is equivalent to a special form of downward continuation for the complex conjugate of the observed magnetic fields. The sources of the migration field are a mirror image (with respect to the observational profile, followed by downward continuation of the complex conjugate of the observed magnetic field data) of the true sources. Physically, the migration field can be obtained by moving the sources of the observed magnetic fields above the observational profile, and by then downward continuation the complex conjugate of the observed magnetic field data. The migration field contains remnant information about the original sources so it can be used for imaging the susceptibility distribution in the subsurface. The remarkable feature of potential field migration is that, contrary to the conventional transforms such as downward continuation or the calculation of higher order derivatives, the method is very stable and produces robust images of subsurface structures. In addition, the method does not require any *a priori* information about the type of the source of the magnetic field. Note that, in both theoretical and field examples we observe the broadening of the high susceptibility zone/region with depth in

the migration images. This property is consistent with the known decrease of the resolution from potential field data.

We have applied our migration to GETMAG magnetic tensor data over a magnetite skarn at Tallawang in New South Wales, Australia; the results of which agree very well with both Euler deconvolution and the known geology. Similar to Zhdanov *et al.* (2011), magnetic migration can be extended to the 3-D case, and this will be the subject of a subsequent paper.

We note in the conclusion that the developed method is also applicable to the vast amounts of high quality conventional magnetic survey data that have been acquired over the last few decades, if those data are processed to calculate vector and tensor data by Fourier processing of TMI measurements.

ACKNOWLEDGMENTS

The authors acknowledge TechnoImaging for support of this research and permission to publish. Zhdanov and Cai acknowledge support of The University of Utah's Consortium for Electromagnetic Modeling and Inversion (CEMI). The authors thank CSIRO Materials Science and Engineering, in particular Drs. Phil Schmidt, Keith Leslie, David Clark and Cathy Foley, for providing the Tallawang GETMAG data and related material.

REFERENCES

- Berkhout, A.J., 1980. *Seismic Migration*, Elsevier, Amsterdam.
- Claerbout, J.F., 1985. *Imaging the Earth's Interior*, Blackwell Scientific Publications, Oxford.
- Foley, C.P. & Leslie, K.E., 1998. Potential use of high Tc SQUIDs for airborne electromagnetics, *Explor. Geophys.*, **29**, 30–34.
- Foley, C.P. *et al.*, 1999. Field trials using HTS SQUID magnetometers for ground-based and airborne geophysical applications, *IEEE Trans. App. Superconductivity*, **9**, 3786–3792.
- Lee, J.B. *et al.*, 2001. Experience with SQUID magnetometers in airborne TEM surveying, *Explor. Geophys.*, **32**, 9–13.
- Rompel, A.K.K., 2009. Geologic applications of FTMG, presented at *11th SAGA Biennial Technical Meeting and Exhibition*, Swasiland.
- Schmidt, P.W. & Clark, D.A., 2006. The magnetic gradient tensor - its properties and uses in source characterization, *The Leading Edge*, **25**, 75–78.
- Schmidt, P., Clark, D., Leslie K.E., Bick, M., Tilbrook, D.L. & Foley, C.P., 2004. GETMAG - a SQUID magnetic tensor gradiometer for mineral and oil exploration, *Explor. Geophys.*, **35**, 297–305.
- Schneider, W.A., 1978. Integral formulation for migration in two and three dimensions, *Geophysics*, **43**, 49–76.
- Stolz, R., Zakosarenko, V., Schulz, M., Chwala, A., Fritzsche, L., Meyer, H.-G. & Kostlin, E.O., 2006. Magnetic full-tensor SQUID gradiometer system for geophysical applications, *The Leading Edge*, **25**, 178–180.
- Tilbrook, D.L., 2004. The design of a new concept HTSC axial gradiometer, *Physica C*, **407**, 1–9.
- Wynn, W.M., Frahm, C.P., Carroll, P.J., Clark, R.H., Wellhoner, J. & Wynn, M.J., 1975. Advanced superconducting gradiometer/magnetometer arrays and a novel signal processing technique, *IEEE Trans. Magn.*, **11**, 701–707.
- Zhdanov, M.S., 1981. Continuation of non-stationary electromagnetic fields in geoelectrical problems, *Izvestia Akademii Nauk SSSR, Fizika Zemli*, **12**, 60–69.
- Zhdanov, M.S., 1988. *Integral Transforms in Geophysics*, Springer-Verlag, Berlin.
- Zhdanov, M.S., 2002. *Geophysical Inverse Theory and Regularization Problems*, Elsevier, Amsterdam.
- Zhdanov, M.S., Liu, X., Wilson, G.A. & Wan, L., 2011. Potential field migration for rapid imaging of gravity gradiometry data, *Geophys. Prospect.*, **59**, 1052–1071.